ELSEVIER

Nuclear Instruments and Methods in Physics Research A 405 (1998) 60–70

NUCLEAR INSTRUMENTS & METHODS IN PHYSICS RESEARCH Section A

Neutron detection efficiency for the measurement of the $^{2}H(e,e'n)\,^{1}H$ cross section

T. Eden[a,b,*], R. Madey[a,b], P. Markowitz[c,1], P.M. Rutt[c,2], B.D. Anderson[a], A.R. Baldwin[a], D. Barkhuff[d], K.B. Beard[b,c,3], W. Bertozzi[e], J.M. Cameron[f], C.C. Chang[g], G.W. Dodson[e], K. Dow[e], M. Farkhondeh[e], J.M. Finn[c], B.S. Flanders[h], C. Hyde-Wright[i,4], W.-D. Jiang[i], D. Keane[a], J.J. Kelly[g], W. Korsch[e,5], S. Kowalski[e], R. Lourie[d], J. McIntyre[c,2], D.M. Manley[a], J. Mougey[j,6], B. Ni[f,7], T. Payerle[g], P.J. Pella[k], T. Reichelt[l], M. Spraker[f,8], D. Tieger[e], W. Turchinetz[e], P.E. Ulmer[j,4], S. Van Verst[d,9], J.W. Watson[a], L.B. Weinstein[e,4], R.R. Whitney[j], W.-M. Zhang[a]

[a] *Kent State University, Kent, OH 44242, USA*
[b] *Hampton University, Hampton, VA 23668, USA*
[c] *The College of William & Mary, Williamsburg, VA 23185, USA*
[d] *University of Virginia, Charlottesville, VA 22904, USA*
[e] *Massachusetts Institute of Technology, Cambridge, MA 02139, USA*
[f] *Indiana University Cyclotron Facility, Bloomington, IN 47408, USA*
[g] *University of Maryland, College Park, MD 20742, USA*
[h] *The American University, Washington DC 20016, USA*
[i] *University of Washington, Seattle, WA 98195, USA*
[j] *Thomas Jefferson National Accelerator Facility, Newport News, VA 23606, USA*
[k] *Gettysburg College, Gettysburg, PA 17325, USA*
[l] *Physikalisches Institut Universität Bonn, D–53115 Bonn, Germany*

Received 10 January 1997; received in revised form 4 August 1997

Abstract

We report a measurement of the neutron detection efficiency for an array of neutron detectors behind a lead-steel wall consisting of 10.16 cm thick lead bricks sandwiched between 3.18 cm steel plates. The neutron detection efficiency ε was

* Correspondence address: TJNAF MS28F, 12000 Jefferson Ave., Newport News, VA 23606, USA. Tel.: + 1 757 7310; fax: + 1 757 269 7559; e-mail: qeden@cebaf.gov.

[1] Present address: Florida International University, Miami, FL 33199, USA.
[2] Present address: Rutgers University, Piscataway, NJ 08855, USA.
[3] Present address: James Madison University, Harrisonburg, VA 22807, USA.
[4] Present address: Old Dominion University, Norfolk, VA 23529, USA.
[5] Present address: New Mexico State University, Las Cruces, NM 88003, USA.
[6] Present address: Centre d'Etudes Nucléaires, Saclay, Gif-sur-Yvette, France.
[7] Present address: Rush University, Chicago, IL 60612, USA.
[8] Present address: Duke University, Durham, NC 27707, USA.
[9] Present address: Washington Department of Health, Olympia, WA 98504, USA.

PII S0168-9002(97)01158-3

obtained from the ratio of coincidence to single-arm proton cross sections using the $\gamma + {}^2_1\mathrm{H} \rightarrow \mathrm{p} + \mathrm{n}$ reaction. Knowledge of the neutron detection efficiency was necessary to extract the cross section for the exclusive ^{2}H(e,e′n)^{1}H reaction, which we used to obtain the elastic magnetic form factor G_M^n of the neutron. The measurements for three different neutron energies were carried out at the MIT-Bates Linear Accelerator Center with an incident electron beam energy of 254 MeV.

PACS: 29.30.Aj; 25.20.-x; 25.10. + s

Keywords: Neutron detection efficiency; Associated-particle technique

1. Introduction

In an earlier paper[1], we reported a measurement of the elastic magnetic form factor G_M^n of the neutron with apparatus developed to measure the electric form factor G_E^n of the neutron [2,3]. In determining G_M^n, we measured the exclusive unpolarized cross section of the ^{2}H(e,e′n)^{1}H reaction. Neutrons were detected with a sequential array of detectors situated inside a large shielding enclosure. The front face of the shielding enclosure consisted of a lead–steel wall, composed of 10.16-cm-thick lead bricks sandwiched between two 3.18-cm-steel plates. The purpose of this lead–steel wall was to attenuate the high-energy photon flux from the target and to shield the detectors against charged particles. A steel collimator, 1-m-thick, was used to shield the rear detectors in the neutron polarimeter from the direct path of neutrons produced at the target. Prior measurements [4] at Bates established the need for substantial shielding of the neutron detectors for both the G_E^n and G_M^n measurements. An illustration of the experimental layout is shown in Fig. 1.

To determine the coincidence cross section for the exclusive ^{2}H(e,e′n)^{1}H reaction, we need the detection efficiency for the neutron arm, which includes the detectors, the lead–steel wall, and the veto counter. The efficiency ε of the neutron arm, which is a function of the incident neutron momentum P_n, is given by the product

$$\varepsilon = T \cdot \varrho, \tag{1}$$

where $T(P_n)$ is the probability that a neutron will be transmitted through the shielding and $\varrho(P_n)$ is the probability that the neutron will interact in one of the elements of the detector array. We determined ε in Eq. (1) by the *associated-particle* technique, which requires the use of a nuclear reaction with a two-body final state; in particular, if we demand that one of the particles produced be a neutron, which is detected in the neutron arm with an unknown efficiency, and the other be an associated charged particle, which is detected in coincidence in a magnetic spectrometer, then the efficiency of the neutron arm is

$$\varepsilon = \frac{\sigma_{\mathrm{coin}}}{\sigma_{\mathrm{single}}}. \tag{2}$$

Here σ_{coin} represents the number of real coincidences between a neutron and a charged particle, and σ_{single} is the number of single-arm charged particle events. In determining σ_{coin} and σ_{single}, we subtract events from the target cell walls to isolate events from liquid deuterium (LD_2).

The particular reaction chosen to investigate the neutron-arm efficiency was the photodisintegration reaction $\gamma + {}^2_1\mathrm{H} \rightarrow \mathrm{p} + \mathrm{n}$. The gamma rays produced in the LD_2 target and used to disintegrate the deuterons are peaked strongly in the forward direction. A mixture of real and virtual (viz., $N(v) = (2\alpha/\pi)\ln(E_e/m_e) \simeq 2.9\%$ [5]) photons with roughly the shape of a thin-target bremsstrahlung spectrum [6] was provided by passing the electron beam through the LD_2 target. Because the electrons are not detected, the two-body final state was selected by detecting protons near to the maximum energy allowed by the electron beam energy, thereby eliminating energetically any pion production from nucleon or nuclear excitations.

Listed in Table 1 are three kinematic points for the detection efficiency measurements at

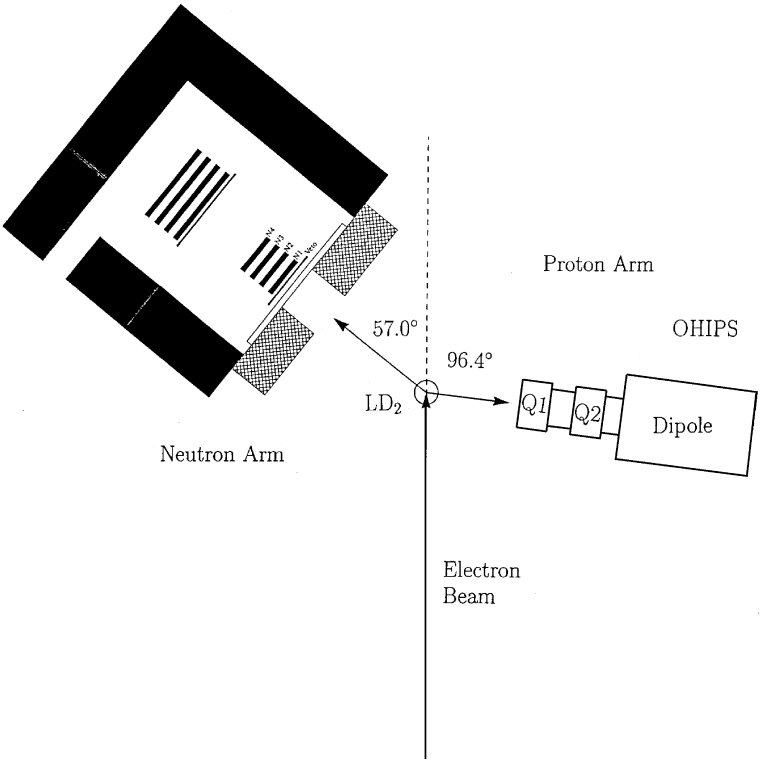

Fig. 1. Plan view of the experimental layout. The shielding for the neutron arm consisted of a collimated steel wall (cross hatched), lead-steel wall (long-unshaded rectangle), and reinforced concrete walls (shaded). The four front neutron detectors (N1–N4) and veto counter are situated behind the lead-steel wall. The proton arm displays the two quadrupole magnets, Q1 and Q2, and the dipole magnet of OHIPS.

Table 1
Kinematics for the ^{2}H(γ,pn) neutron-arm detection efficiency measurements at $E_{beam} = 254$ MeV and $\theta_n = 57^\circ$

E_γ (MeV)	T_n (MeV)	P_n (MeV/c)	T_p (MeV)	P_p (MeV/c)	θ_p (deg)
116.5	65.0	355.5	51.5	308.0	−104.5
165.7	94.0	430.7	71.7	367.7	−100.8
235.3	135.0	521.4	100.3	440.0	−96.4

$E_{beam} = 254$ MeV. The incident electron beam had an average beam current of ~ 1.25 μA, and a duty factor of 0.8%. The neutron energies chosen were based on three different squared four-momentum transfer (Q^2) points that were examined experimentally to obtain G_M^n from the quasielastic ^{2}H(e,e′n)^{1}H reaction.

2. Experimental arrangement

2.1. Cryogenic target

The LD_2 target was a cylinder (5 cm diameter) with a thickness of 0.81 g/cm^2 (= 0.66% radiation length). The LD_2 target cell was oriented with its cylindrical axis perpendicular to the direction of the beam. The target cell walls were constructed of a metallic alloy Elgiloy (*A trademark of the Elgin Watch Co.) with a density of 8.369 g/cm^3. The chemical composition of this alloy is 40% cobalt, 20% chromium, 15.9% iron, 15% nickel, 7% molybdenum, 2% manganese, and 0.1% carbon. The walls of the target cell were 5.08×10^{-3} cm (= 42.5 mg/cm^2) thick; the ratio of the mass of deuterium to Elgiloy was $\sim 10:1$. The radiation

length of the Elgiloy walls was about 0.31%. Because the target was pressurized to 276–414 kPa, the outer diameter of the target cell increased by 0.018 ± 0.003 cm, giving an inner diameter of 5.062 ± 0.005 cm [7]; however, because we measured a ratio of cross sections, target normalizations were not needed.

The target was cooled by circulating liquid helium through copper coils located at the top surface of the target. To monitor the target temperature, carbon–glass resistors were located at the bottom of the target cell. An independent computer control system regulated the pressure and temperature of the target. A schematic illustration of the target cell is shown in Fig. 2.

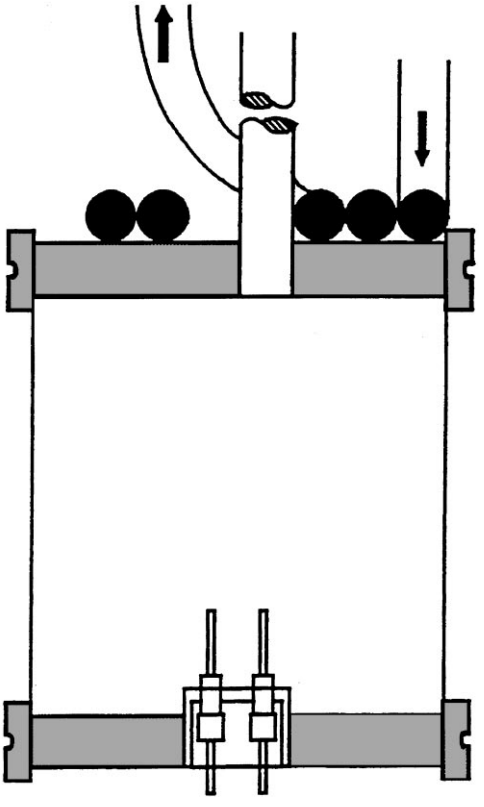

Fig. 2. A side view of the cryogenic target. The beam would pass (left to right) through the central portion of the 5 cm-diameter chamber. Note the carbon-glass resistors at the bottom of the cell.

2.2. Proton arm

Protons were detected in the magnetic spectrometer OHIPS (the one hundred inch proton spectrometer) at various angles (see Table 1) to the right of the incident beam. OHIPS is a QQD (quadrupole–quadrupole–dipole) spectrometer. The spectrometer and its focal-plane instrumentation are discussed in detail by Turley [8].

The actual measurements of the particle position and angle, which were used for determining the particle trajectory through the spectrometer, were performed by processing the signals from two planes of wires in the vertical-drift chamber (VDCX) in OHIPS. The two planes were aligned at 45° with respect to a central trajectory through the spectrometer. Each plane had 104 wires spaced 4.23 mm apart. Viewed in the x–y plane, the two wire planes inside the VDCX volume were configured at 45° and 135° with respect to the x-axis, respectively. The OHIPS VDCX was read out by the use of a conventional delay-line system [9]. This delay-line system was a primary component in reconstructing the track of a proton through the spectrometer.

2.3. Neutron arm

The front detector array of the neutron polarimeter (for measuring G_E^n) was utilized to detect neutrons emitted from the target. This front detector array consisted of four mineral-oil (BC-517L) scintillation counters, each with dimensions of 0.254-m high $\times$ 0.508-m long $\times$ 0.102-m thick; the array was situated at a mean flight path of 3.63 m from the target and at a neutron scattering angle $\theta_n = 57°$. Ahead of the front detector array was a thin (0.953-cm thick) plastic scintillation counter to veto charged particles. These neutron detectors provided ample solid-angle coverage to detect any neutron that was correlated with a proton; for instance, at the $Q^2 = 0.255$ $(\mathrm{GeV}/c)^2$ point, neutrons illuminated $\sim 34\%$ ($\sim 44\%$) of the front-most neutron detector (rear-most neutron detector).

The shielding enclosure that housed the neutron polarimeter was composed of a 1-m-thick front steel wall with a 26.7-cm high $\times$ 65.8-cm wide collimated opening; a lead–steel wall located

immediately behind the collimated opening (ahead of the polarimeter) was made up of 10.16-cm lead bricks sandwiched between two 3.18-cm steel plates. The rest of the shielding enclosure consisted of 122-cm-thick walls and a 61-cm-thick roof of reinforced high-density ($\rho = 3.9$ g/cm^3) concrete. A narrow concrete labyrinth at the rear of the enclosure was used to enter and exit the housing.

3. Experimental procedure

An unpolarized electron beam was incident on an unpolarized LD_2 target; neutrons and protons were detected separately (prescaled) and in coincidence. A separate trigger from each arm was required to generate a two-arm coincidence trigger.

3.1. Neutron single-arm trigger

The neutron single-arm trigger was created from a mean-timed signal in the neutron detector array. The associated mean-timed detector electronics have been described elsewhere [10]. Coupled to a light pipe at the end of each neutron detector was a 5-in-diameter Philips XP-2041 photomultiplier tube (PMT). The signal cable carries the output signal from the anode of the PMT to various NIM modules and eventually to an analog mean-timer circuit. With this configuration of electronics, we measured (1) the time-of-flight (TOF) of a neutron from the target to one of the front scatterers with a start signal from the proton arm (see Section 3.3.), (2) the position of interaction in the detectors participating in an event, and (3) the pulse height from those detectors. Shown in Fig. 3 is a block diagram of a neutron detector and the associated mean-timed electronics used for this experiment.

The mean-timed signals from the neutron detectors participating in an event were discriminated before being delivered to CAMAC TDC modules, scaler modules, and to a coincidence module input where the neutron single-arm trigger was generated. The hardware threshold settings for the constant-fraction discriminators were ~ 1.5 MeVee (MeV of equivalent–electron energy) for the front-most neutron detector N1 and ~ 1.0 MeVee for the other three neutron detectors N2, N3, and N4. Mean-timed signals were sent also to CAMAC ADCs enabling the acquisition of pulse-height information for each neutron detector event-by-event.

3.2. Proton single-arm trigger

The proton single-arm trigger utilized analog signals from three detectors (after the VDCX) in the spectrometer scintillator array. Signals from these scintillators, which were delivered to the counting room on 90 Ω cables, provided timing information and the fast-trigger logic. The mean-timed signals from two of the scintillators (S0 and S1) along with the signal from a paddle scintillator (S2) were sent to a majority-logic unit (MLU). A three-fold coincidence of the three scintillator signals was demanded by the MLU to initiate the proton single-arm trigger.

3.3. Coincidence trigger

The coincidence trigger was generated by the proton single-arm trigger in coincidence with the neutron single-arm trigger. The time window was about 120 ns wide. The resulting coincidence pulse is timed from the proton single-arm trigger and was used to start the neutron detector TOF TDCs. A second signal, retimed from the neutron trigger, enabled the logic required to retain the position and pulse-height data from the neutron arm. A similar signal in the proton arm allowed for single-arm data (ADCs and TDCs) in OHIPS to be acquired; therefore, the timing of these coincidence-gated single-arm triggers reflected the timing of the single-arm triggers. These single-arm triggers were limited to one event per beam burst by a gate and delay circuit.

Besides recording coincidence events, "prescaled" single-arm acquisition was implemented during this experiment. The prescaling factor determined the fraction of single-arm events written to tape. These events were selected by forming a logical AND between the single-arm trigger and a pulse generator with an adjustable rate in the "prescaler". For this experiment, the prescale fraction was set at 1 : 1.

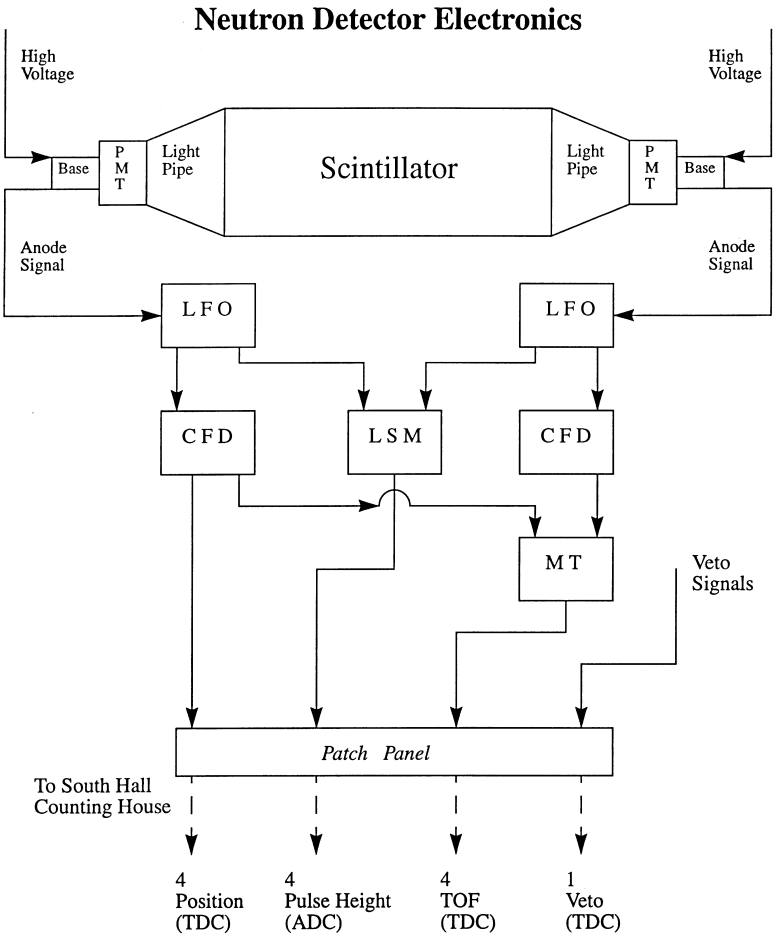

Fig. 3. Schematic diagram of a mean-timed neutron detector with associated electronics for generating TOF, pulse-height, and position signals. The abbreviated symbols represent the following NIM electronics modules: linear fanout (LFM), constant-fraction discriminator (CFD), linear summing (LSM), and mean timer (MT).

3.4. Instrumental calibrations

Calibration constants were required for both arms to analyze properly the data that were written to tape. Madey et al. [11] describe the techniques for obtaining the position calibration, pulse-height calibration, and intrinsic time dispersion for large-volume, mean-timed organic scintillator detectors for neutrons. The intrinsic time dispersion includes only contributions from light collection and neutron detector electronics.

To insure proper reconstruction of proton tracks through the VDCX in OHIPS, delay-line calibrations were performed for each run. These calibration constants (slopes and offsets) were useful to identify ordered hits in each wire layer. From these ordered hits in both layers, one can discern a "good" track in an off-line analysis, which was needed in both the single-arm and coincidence analyses.

4. Data analysis

Shown in Fig. 4 is a coincidence TOF spectrum from the ^{2}H(γ,pn) reaction at a central neutron kinetic energy $T_n = 135$ MeV. This spectrum,

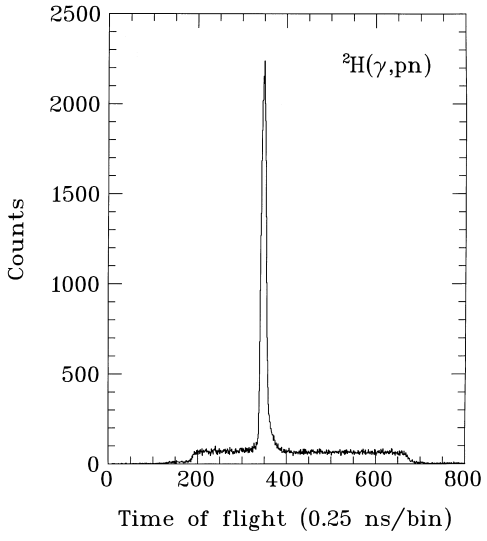

Fig. 4. A summed TOF spectrum, at hardware thresholds, from the ^{2}H(γ,pn) reaction at a central neutron kinetic energy, $T_n = 135$ MeV. The coincidence signal between the neutron and proton arms sits above a sea of accidental coincidences.

which is the sum of the TOF spectra from all four front detectors, was generated before any software cuts were imposed. The spectrum is a time difference between the proton arm and the neutron arm; i.e., a proton single-arm trigger generates the TDC start signal while an event in a detector of the neutron arm generates a TDC stop. The width of the spectrum (~ 480 channels $\times$ 0.25 ns/channel $= 120$ ns) was the window for accepting coincidence events between the proton arm and the neutron detector. Contributions to the width of the coincidence peak in the spectrum included the beam-energy spread, the time dispersion through the magnetic spectrometer, and the intrinsic time dispersion of the neutron-detector system. The peak is sitting on a background of accidental (or chance) coincidences which were generated by neutrons at the target that were not correlated in time with a proton. The indicated background level is flat and was useful in extracting the real-event signal above background.

Shown in Figs. 5–7 are histograms recorded in OHIPS of the momentum of protons from deuterium photodisintegration by bremsstrahlung, the optical traceback of a filled LD_2 target, and the optical traceback of an empty LD_2 target cell, respectively. The empty-target-cell histogram displayed in Fig. 7 reveals the cell walls which were reconstructed by optical trace back from the focal plane in OHIPS to the position of the target cell.

4.1. Data sorting

Criteria for determining a "good" neutron to be used in the analysis of single-scattering events were as follows:

1. A detected neutron must register an ADC value above a given software pulse-height threshold. These thresholds were determined from pulse-height calibrations taken before and after the data runs. From the calibration points for each detector, a linear least-squares fitting program is used to calculate a *best-fit* straight line through the calibration data. Calibration spectra from all four detectors are shown in Fig. 8. The uncertainties from the slope and offset for each fit contribute to the systematic uncertainty in determining the neutron-arm efficiency.
2. A neutron must appear within the 120 ns TDC coincidence time window. All underflows and overflows are discarded.
3. Charged-particle events were not actively vetoed during data-acquisition mode; however, we recorded a TDC spectrum of the veto counter that allowed for an off-line vetoing of these charged-particle events. Any registered neutron events that had a simultaneous event appearing in the veto TOF spectrum was discarded. The dead-time in the data-acquisition system was negligible ($\leq 1\%$), with and without the veto in the neutron single-arm trigger.

These three tests provided the criteria for a "good" single-arm neutron. A "good" single-arm proton must have three or four ordered hits in both wire planes with a reconstructed track. Although a CO_2 gas Čherenkov detector was part of the detector stack in OHIPS during the experiment (used for e^-/π^- particle identification for the G_E^n experiment), positively identifying protons was not an issue because pion production was suppressed kinematically. Shown in Fig. 9 is a summed coincidence TOF spectrum after the above

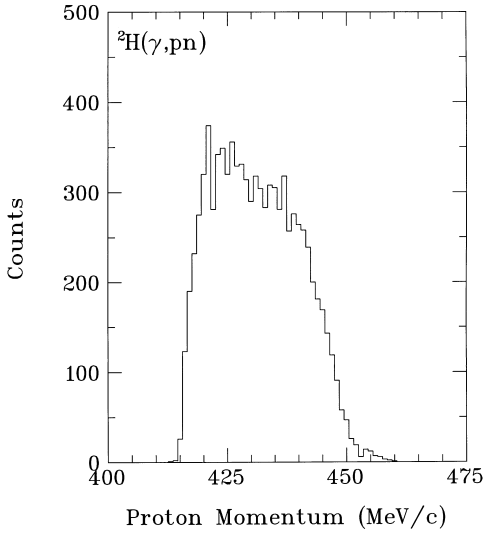

Fig. 5. Reconstructed momentum spectrum of protons from deuterium photodisintegration by bremsstrahlung, for the data point at $T_n = 135$ MeV.

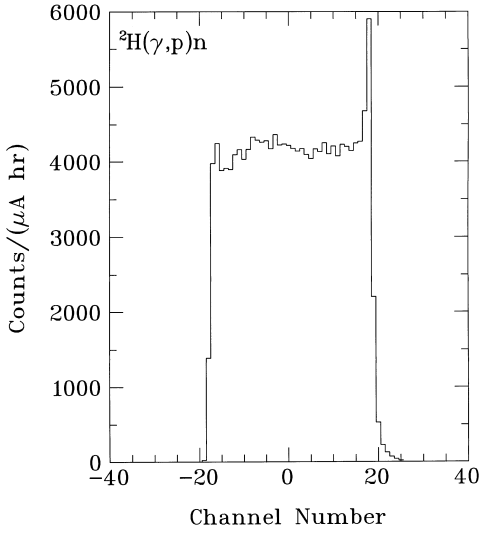

Fig. 6. Optical traceback histogram of filled LD_2 target cell, for the data point at $T_n = 65$ MeV.

software conditions were imposed for a neutron energy of 135 MeV.

4.2. Peak fitting

From the output of the data-sorting routine (Fig. 9), we proceeded to extract σ_{coin}. To obtain the

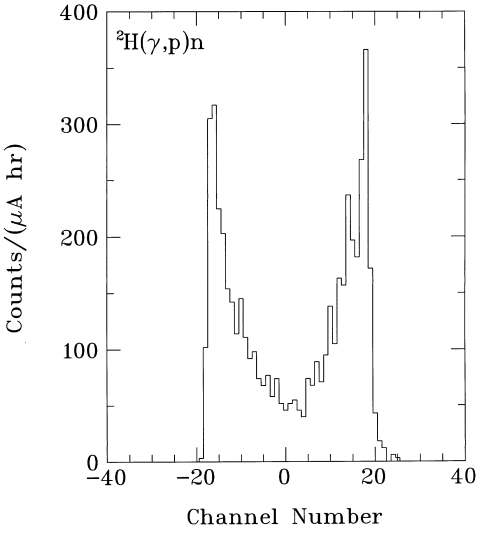

Fig. 7. Optical traceback histogram of empty LD_2 target cell, for the data point at $T_n = 65$ MeV.

number of counts above background, we used the minimization program MINUIT[12] to fit the peak and the background in Fig. 9. Because of the exponential tail on the right-hand side of the TOF peak, an ordinary asymmetric Gaussian fit is unsatisfactory to extract the counts above background. Instead, a minimum χ^2 was achieved by using the following functional form for the coincidence peak:

$$y(x) = A \exp\left[-\frac{1}{2}\left(\frac{x-\mu}{\sigma_1}\right)^{\gamma}\right], \quad x \le \mu \tag{3}$$

$$y(x) = A \exp\left[-\frac{(x-\mu)}{\sigma_2}\right], \quad x > \mu \tag{4}$$

Here μ is the mean, γ is the exponent, σ_1 and σ_2 are the left and right standard deviations of the fitted distribution, respectively, and A is the amplitude of the peak above background. The background is fitted with a first-order polynomial for all x. Shown in Fig. 10 is a typical fit to the coincidence TOF spectrum for the $T_n = 65$ MeV point at a pulse-height threshold of 4 MeVee.

5. Results

For each neutron energy, neutron-arm efficiencies were extracted at four different neutron

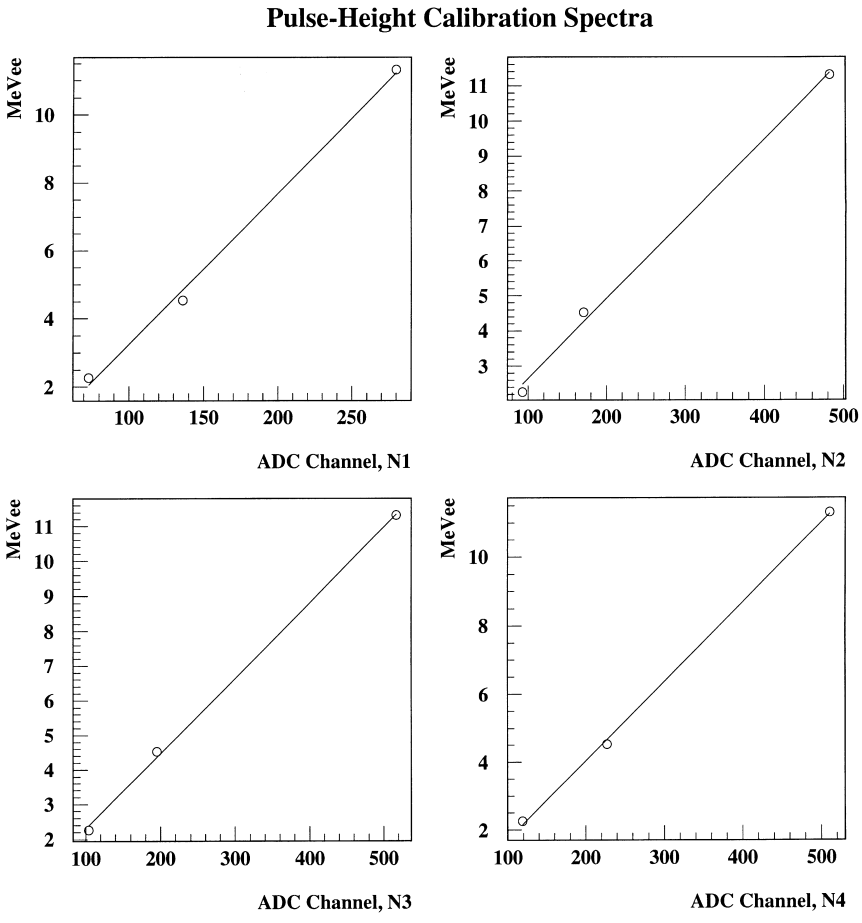

Fig. 8. Plots of the fitted pulse-height calibration curves to the calibration data for each neutron detector. The open circles are the calibration data points taken with a radioactive ^{228}Th γ-ray source.

detector pulse-height thresholds: 2, 4, 6, and 8 MeVee. Shown in Table 2 are the extracted neutron-arm detection efficiencies for each central neutron energy examined during the experiment. Also listed in Table 2 is the neutron transmission $T(P_n)$ through the shielding. The error shown is statistical only; it was calculated from the expression given below

$$\frac{\Delta\varepsilon}{\varepsilon} = \left[\left(\frac{\Delta\sigma_{\text{coin}}}{\sigma_{\text{coin}}}\right)^2 + \left(\frac{\Delta\sigma_{\text{single}}}{\sigma_{\text{single}}}\right)^2\right]^{1/2}. \quad (5)$$

The uncertainty $\Delta\varepsilon$ in Eq. (5) is dominated by the contribution from $\Delta\sigma_{\text{coin}}$, which is determined from fitting the coincidence TOF peak to obtain the yield above background. In extracting ε, we normalized all cross sections to counts/(μA h). Also, the single-arm cross sections for each measurement were corrected for events produced from interactions in the target cell walls; the corrections were on the order of 10% and contributed a negligible amount to $\Delta\varepsilon$. Coincidence events from the target cell walls were negligible. Empty target cell runs were performed at each energy to obtain both single-arm and coincidence cross sections, allowing for a normalized subtraction to obtain the separated LD_2 cross sections. A plot of the neutron-arm efficiency versus neutron kinetic energy is shown in

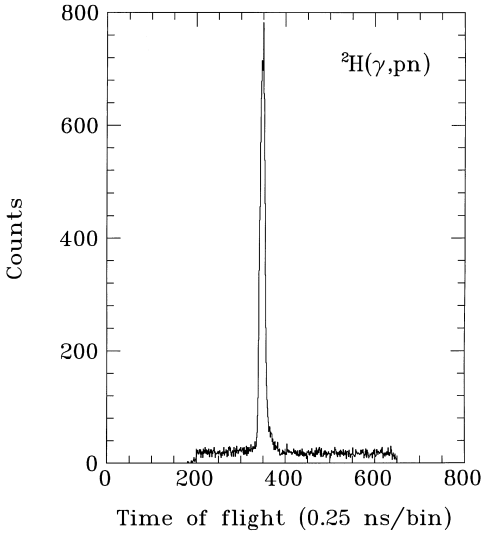

Fig. 9. Final coincidence TOF spectrum for the data point at $T_n = 135$ MeV.

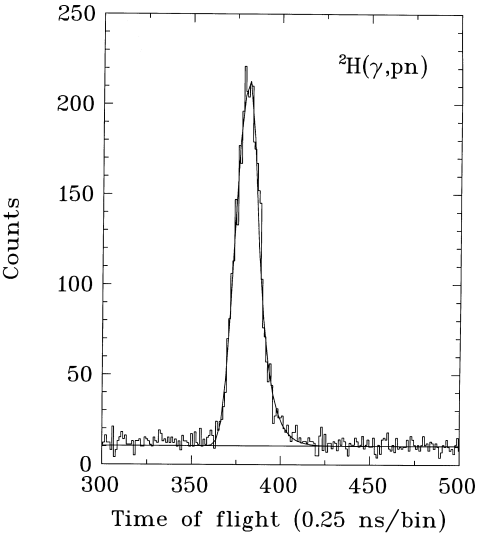

Fig. 10. Typical fit to a coincidence TOF spectrum.

Fig. 11 results for a pulse-height threshold of 4 MeVee.

6. Conclusions

We used the associated-particle technique to obtain neutron detection efficiencies for three different neutron energies. Knowledge of the neutron detection efficiency was necessary to extract the unpolarized cross section for the exclusive ^{2}H(e,e′n)^{1}H reaction, which was used to obtain the Sachs elastic magnetic form factor G_M^n of the neutron. For a 4 Me Vee threshold, the efficiency ε varied from $(4.83 \pm 0.21)\%$ at $T_n = 65$ MeV, to $(5.93 \pm 0.37)\%$ at $T_n = 94$ MeV, to $(7.31 \pm 0.18)\%$ at $T_n = 135$ MeV.

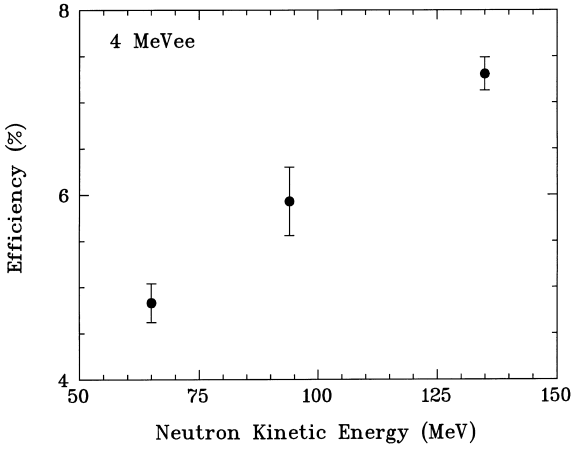

Fig. 11. Efficiency as a function of neutron kinetic energy for a pulse-height threshold of 4 MeVee. The error bars are the same as those listed in Table 2.

Table 2
Neutron-arm detection efficiencies at various pulse-height threshold settings for the three neutron energies examined. The uncertainties ΔT_n were calculated from the observed proton energy spread and kinematics for each Q^2 point

$T_n \pm \Delta T_n$ (MeV)	$T(P_n)$	ε (%) (@ 2 MeVee)	ε (%) (@ 4 MeVee)	ε (%) (@ 6 MeVee)	ε (%) (@ 8 MeVee)
65.0 ± 1.3	0.26	4.86 ± 0.21	4.83 ± 0.21	4.61 ± 0.20	4.24 ± 0.19
94.0 ± 2.8	0.33	6.14 ± 0.38	5.93 ± 0.37	5.60 ± 0.34	5.22 ± 0.23
135.0 ± 3.6	0.39	7.33 ± 0.18	7.31 ± 0.18	7.19 ± 0.18	6.87 ± 0.19

Good coincidence count rates and a large signal-to-noise ratio makes the associated-particle technique a fast and easy way to measure the efficiency of a neutron detector and its related shielding in the radiation environment of an electron accelerator.

Acknowledgements

We thank the Bates staff for their help during all stages of this experiment. This research was supported in part by the National Science Foundation under Grant Nos. HRD-9633750, HRD-9154080, PHY-95-13924, PHY-91-07064, PHY-91-12816, PHY-89-02479, PHY-88-02392, PHY-86-58127, PHY-86-15512, PHY-85-01054, the Department of Energy under Grant Nos. DE-FG05-90ER40570, DE-FG06-90ER40537, DE-FG02-89ER40531, DE-AC05-84ER40150, DE-AC02-76ER03069, and by grants from the Deutsche Forschungsgemeinschaft (SFB 201 and RE 791/1-1).

References

[1] P. Markowitz et al., Phys. Rev. C 48 (1993) R5.
[2] T. Eden et al., Phys. Rev. C 50 (1994) R1749.
[3] T. Eden et al., Nucl. Instr. and Meth. A 338 (1994) 432.
[4] R. Madey et al., in 1987–1988 Annual Scientific and Technical Report, Bates Linear Accelerator Center, pp. 140-156
[5] R.H. Dalitz, D.R. Yennie, Phys. Rev. 105 (1957) 1598.
[6] J.L. Matthews, R.O. Owens, Nucl. Instr. and Meth. 111 (1973) 157.
[7] M. Farkhondeh, unpublished, 1992.
[8] R.S. Turley, Ph.D. Dissertation, MIT, 1984.
[9] W. Bertozzi et al., Nucl. Instr. and Meth. 141 (1977) 457.
[10] A.R. Baldwin, R. Madey, Nucl. Instr. and Meth. 171 (1980) 149.
[11] R. Madey et al., Nucl. Instr. and Meth. A 214 (1983) 401.
[12] F. James, M. Roos, Comp. Phys. Commun. 10 (1975) 343.